A theoretical model of transient cyclic voltammetry for electroactive biofilms

Raphaël Rousseau, Marie-Line Délia-Dupuy, Alain Bergel

A theoretical model of transient cyclic voltammetry for electroactive biofilms

DOI: 10.1039/c3ee42329h

Raphael Rousseau, Marie-Line Délia and Alain Bergel*

A numerical model is designed to model transient cyclic voltammetry (CV) on electroactive biofilms. The dependence of the transient current peak (J_{peak}) on the potential scan rate (v) is approached through a power law (J_{peak} *vs.* v^{α}) as is usually done in experimental studies. The two straightforward rules of thumb ($\alpha = 1$ or $\alpha = 0.5$), which are the only theoretical tools available so far, are shown to be partly deficient. In contrast, the model explains the fact that the α exponent can vary in a large range of values from 1 to 0.34 (possibly lower), as observed in experimental studies, and gives theoretically supported rules for interpreting transient CV of electroactive biofilms.

Broader context

It has recently been realized that some microorganisms can be efficient electro-catalysts in electrochemical processes. Consequently, the domain of microbial electrochemical technologies (microbial fuel cells, microbial electrolysis cells, microbial electrosynthesis cells *etc.*) has been developing extremely fast for around 10 years, with very promising applications in a wide variety of fields such as the production of renewable energy, waste treatment, bioremediation and electrosynthesis. New electron transfer pathways between microorganisms and electrodes have been discovered, but much remains to be improved in our fundamental understanding. In particular, no theoretical support has been available so far to explain some unexpected experimental behaviours observed through transient cyclic voltammetry. This work develops a theoretical model that was lacking to allow the groups working in the field to powerfully exploit transient electroanalysis of microbial systems.

1. Introduction

Biofilm electroactivity has been studied for a long time in the field of microbial corrosion[1–3] but it became the subject of great interest around ten years ago with the revival of microbial fuel cells and the emergence of several other related technologies such as microbial electrolysis and microbial electrosynthesis.[4–6] The electron transport and transfer mechanisms occurring in electroactive (EA) biofilms have been investigated in considerable depth through experimental and theoretical approaches and cyclic voltammetry (CV) is now used almost routinely in this research domain.

CV can be recorded under two different conditions: catalytic conditions, when the substrate is present in solution and non-turnover conditions in the absence of a substrate. Catalytic CVs are generally performed in stationary mode only, *i.e.* with a potential scan rate low enough for metabolic reactions, mass transfer and electron transport/transfer steps to balance each other. Experimentally, a scan rate of around 1 mV s^{-1} is most often used to ensure such a condition. The stationary catalytic CVs give the current that the electrode can provide over the whole range of scanned potentials and thus provides a complete description of the bioanode performance. Stationary catalytic CVs have been interpreted through the Nernst–Monod equation,[7] which requires only one parameter to be adjusted, or through the Butler–Volmer–Monod equation, which involves five adjustable parameters.[8] The first derivative of the CV curves is increasingly being used to differentiate different electrocatalytic ranges.[9–13] A comprehensive theoretical study has recently reported the analysis of the stationary catalytic CV of EA biofilms.[14,15] The different processes of electron production and electron transport and transfer that occur in a EA biofilm were modelled according to five different steps: substrate mass transfer, metabolic oxidation of the substrate, electron release from the cell to the biofilm electron transport network, electron transport in the biofilm, and Nernstian electron transfer to the electrode. Different CV patterns were identified depending on which of the five steps was rate-limiting. Thanks to this work, it is possible to gain insight into EA biofilm mechanisms from the analysis of the general shape of stationary catalytic CV curves.

Non-turnover conditions suppose that the substrate is no longer present in solution. CV consequently involves only the redox compounds that are present in the biofilm and possibly in the bulk solution, in the absence of any metabolic regeneration. Non-turnover CVs are generally recorded in transient state, except when a large amount of redox mediator has accumulated in solution. In this case, the presence of a significant amount of redox compound in the bulk can ensure a pseudo-stationary

Laboratoire de Génie Chimique CNRS-Université de Toulouse (INPT), 4 allée Emile Monso BP 84234, 31432 Toulouse, France. E-mail: alain.bergel@ensiacet.fr; Fax: +33 5 34 32 36 97; Tel: +33 5 34 32 36 73

state (from a rigorous theoretical point of view, no stationary state is possible for batch electrolysis, but a pseudo-stationary state is most generally obtained experimentally, particularly when a small electrode surface area is used in a large volume of solution). Non-turnover CVs are widely used to differentiate the various redox systems that make up the electron transport systems of EA biofilms.[16,17] For instance, up to seven oxidation peaks have thus been observed, each attributed to a different redox system, for microbial anodes made of *Geobacter sulfurreducens*.[9]

Non-turnover CVs are commonly implemented by recording CV curves at different potential scan rates and then plotting the current peaks (J_{peak}) *versus* the scan rate (v). It is classically known in the field of electroanalysis that a diffusion-limited process gives a J_{peak} *vs.* v^{α} relationship with the α exponent equal to 0.5, while a monolayer of adsorbed redox species leads to α equal to 1. From these established rules, it has often been claimed that $\alpha = 0.5$ identifies a diffusion-limited electron transport, while $\alpha = 1$ indicates electron transport *via* immobilized redox mediators. The precise value $\alpha = 0.5$ has sometimes been obtained experimentally for EA biofilms.[18–20] Other experimental studies have reported J_{peak} *vs.* v^{α} variation fitting neither $\alpha = 0.5$ nor $\alpha = 1$,[21] or leading to intermediate values, for instance, $\alpha = 0.7$.[18] No obvious explanation has been found so far for behaviours deviating from the two theoretically identified values of α.

While many experimental studies use CV, the theoretical analysis of the transient response remains under-utilized in the EA biofilm area. Under catalytic conditions, theoretical support exists for the stationary CV only and, experimentally, the transient catalytic CV is rarely used. Under non-turnover conditions, transient CV is widely used experimentally, but theoretical support is lacking to interpret the data. The two rules of thumb with $\alpha = 1$ or $\alpha = 0.5$ cannot explain the diversity of the α values that have been reported experimentally.

In this context, the purpose of this work was to design a theoretical model for transient CV of EA biofilms. Both non-turnover and catalytic conditions are considered. The biophysical description, which was developed for stationary conditions[14,15] involving diffusion-like electron transport in the biofilm, Nernstian electron transfer with the electrode and coupled metabolic reactions, is implemented here in transient mode. As is generally done, equations are written for a bioanode but a biocathode would lead to identical conclusions provided that the basic electron transfer mechanisms are similar. To the best of our knowledge, the present study is the first theoretical foray into transient CV of EA biofilms. It shows that a large variety of values can be explained for the α exponent and simple rules are extracted to exploit transient CV more powerfully in EA biofilm investigations.

2. Back to basics: analytical solutions

2.1 Semi-analytical relationship ($J_{peak} \div v^{1/2}$) derived from the semi-infinite diffusion model

Generally, for the sake of simplicity, a single redox reaction is considered, which does not involve a stoichiometric change between the reduced and oxidized forms:

$$\mathrm{Red} \leftrightarrow \mathrm{Ox} + ne^{-} \tag{1}$$

Both the oxidized and reduced species are assumed to diffuse freely in the solution:

$$\frac{\partial[\mathrm{Red}]}{\partial t} = D_{\mathrm{Red}} \frac{\partial^2[\mathrm{Red}]}{\partial x^2} \tag{2}$$

$$\frac{\partial[\mathrm{Ox}]}{\partial t} = D_{\mathrm{Ox}} \frac{\partial^2[\mathrm{Ox}]}{\partial x^2} \tag{3}$$

On the electrode surface, the electron transfer rate is assumed to be fast enough to ensure the Nernst equilibrium (reversible system) between reduced and oxidized forms at all times:

$$E = E^{0\prime} + \frac{RT}{nF} \ln\left(\frac{[\mathrm{Ox}]_{x=0}}{[\mathrm{Red}]_{x=0}}\right) \tag{4}$$

where E is the potential of the electrode, $E^{0\prime}$ is the formal potential of the redox system, $[\mathrm{Ox}]_{x=0}$ and $[\mathrm{Red}]_{x=0}$ are the concentrations of the oxidized and reduced species, respectively, at the electrode surface. The concentration ratio at the electrode surface ($x = 0$) is thus controlled by the applied potential E:

$$\frac{[\mathrm{Ox}]_{x=0}}{[\mathrm{Red}]_{x=0}} = \exp\left(\frac{nF(E - E^{0\prime})}{RT}\right) \tag{5}$$

The partial derivative eqn (2) and (3) are difficult to solve in the case of cyclic voltammetry because the linear variation of the applied potential with time:

$$E = E_{\mathrm{ini}} + vt \tag{6}$$

where E_{ini} is the initial value and v is the scan rate (V s^{-1}), results in a complex time-varying boundary condition at the electrode surface:

$$\frac{[\mathrm{Ox}]_{x=0}}{[\mathrm{Red}]_{x=0}} = \exp\left(\frac{nF(E_{\mathrm{ini}} - E^{0\prime} + vt)}{RT}\right) \tag{7}$$

Historically, the hypothesis of semi-infinite diffusion allowed helpful simplification at a time where numerical modelling was in its infancy. This hypothesis assumes that any species can diffuse in the infinite space in front of the electrode surface (Fig. 1A). At the initial time ($t = 0$), the oxidized and reduced species have uniform concentrations in this semi-infinite space and it is assumed that these concentrations remain unchanged with time at an infinite distance from the electrode surface ($x \rightarrow \infty$). A boundary condition required to solve eqn (2) and (3) is thus pushed towards infinity, which allows a semi-analytical expression be found for the CV curves. Even so, this solution requires a pretty cumbersome mathematical treatment, which is detailed in handbooks,[22] to obtain the variation of the current density J with the applied potential E (CV curve) and, finally, the current density peak J_{peak} as a function of the potential scan rate:

$$J_{peak} = 2.69 \times 10^5 n^{3/2} D_{\mathrm{Ox}}{}^{1/2} [\mathrm{Red}]_{t=0}\, v^{1/2} \tag{8}$$

This equation is valid at 25 °C for J_{peak} in A cm^{-2}; D_{Red} is the diffusion coefficient of the oxidized species, in cm^2 s^{-1}; $[\mathrm{Red}]_{t=0}$

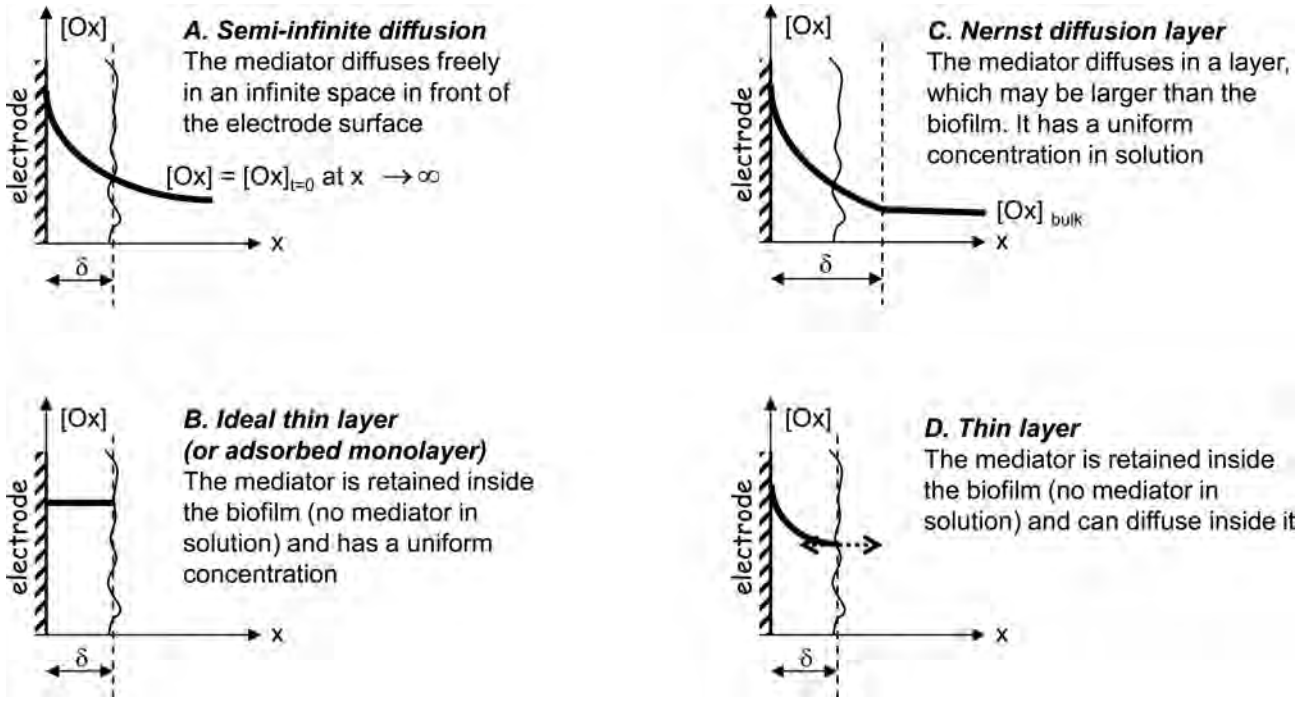

Fig. 1 Scheme of the hypotheses used to model electron transport in an electroactive biofilm.

is the initial concentration of the reduced species, in mol cm^{-3}, and the initial concentration of the oxidized species is equal to zero. In this framework of hypotheses, the peak current density is proportional to the square root of the potential scan rate.

2.2 Analytical relationship ($J_{peak} \div v^1$) derived from the ideal thin layer or adsorbed monolayer model

The thin layer model, symmetrically different from the semi-infinite one, assumes that the redox compound behaves uniformly in a thin layer in contact with the electrode surface. The layer is assumed to be so thin that there is no concentration gradient inside it (and so no diffusion process). Each species has a uniform concentration in the layer (Fig. 1B). This hypothesis is perfectly appropriate when the redox system consists of an adsorbed monolayer of redox compound. It is also used with the so-called thin layer electrochemical cells, which are designed with an electrode facing a very thin layer of solution with a thickness typically in the 2 to 100 μm range.[23] As the concentrations of the oxidized and reduced species are uniform in the layer eqn (7) can be transformed to:

$$\frac{[\mathrm{Ox}]}{[\mathrm{Red}]} = \exp\left(\frac{nF(E_{\mathrm{ini}} - E^{0\prime} + vt)}{RT}\right) \quad (9)$$

The current density is given by the variation of the amount of oxidized species that is produced (or the amount of reduced species that is consumed) with time:

$$J = nF\delta\frac{\partial[\mathrm{Ox}]}{\partial t} = -nF\delta\frac{\partial[\mathrm{Red}]}{\partial t} \quad (10)$$

where δ is the thickness of the thin layer. Solving these equations leads to the variation of J with the applied potential (CV curve), the derivative of which with respect to the potential gives the current density peak:

$$J_{\mathrm{peak}} = \frac{n^2F^2\delta}{4RT}[\mathrm{Red}]_{t=0}v \quad (11)$$

Eqn (11) indicates that J_{peak} is proportional to the potential scan rate v.

This reminder of the accurate framework related to each model points out that the conclusions commonly extracted from eqn (8) and (11) should be qualified. Actually, the two models were designed on the basis of very different hypotheses: the semi-infinite diffusion model assumes a redox compound freely diffusing in a semi-infinite space, while the ideal thin layer (or adsorbed monolayer) model is based on a layer so thin that no concentration gradient occurs inside it. The conclusions that can be justifiably extracted from these two approaches are:

- a redox compound able to diffuse in a "very large solution space" gives J_{peak} proportional to $v^{1/2}$,
- a redox compound confined inside an "ideal thin layer" in contact with the electrode surface leads to J_{peak} proportional to v.

The question to be addressed now is to what extent a "very large solution space" or the "ideal thin layer" can approach what actually occurs in EA biofilms?

3. Nernst diffusion layer and thin layer models to model electron transport in EA biofilms: non-turnover CV

3.1 Modelling electron transport in EA biofilms

Various pathways have been identified for electron transport through EA biofilms. Electrons can be transported to the

electrode surface through the physical diffusion of soluble extracellular mediators, *e.g.* phenazines,[24] thionine,[25] flavin,[26] *etc.*, which are produced by the cells. They can also follow a chain of successive reduction/oxidation reactions between adjacent bound mediator molecules. In this case, electrons move through the biofilm by hopping from a reduced molecule to a neighbouring oxidized one (case of a bioanode). The conductive nature of the biofilm matrix has been shown by several studies[27–29] and electron hopping between outer-membrane cytochromes and/or linked redox enzymes has often been claimed.[30,31] Electron hopping was first described and theorized for chemically modified electrodes, in which electroactive groups were attached to the electrode-bound film. It has been modelled *via* a common diffusion step using an apparent diffusion coefficient representing diffusion-like transport of electrons.[22] In consequence, electron transport through EA biofilms can be modelled as a whole by a diffusion step with an apparent diffusion coefficient D_{app} that includes the different transport mechanisms, either *via* diffusion of a soluble mediator or by electron hopping. This global approach is used here.

Electron transfer through the EA biofilm is modelled with an apparent diffusion coefficient D_{app}, which is assumed to be identical for the reduced and oxidized species:

$$\frac{\partial[\mathrm{Red}]}{\partial t} = D_{app}\frac{\partial^2[\mathrm{Red}]}{\partial x^2} \tag{12}$$

$$\frac{\partial[\mathrm{Ox}]}{\partial t} = D_{app}\frac{\partial^2[\mathrm{Ox}]}{\partial x^2} \tag{13}$$

Assuming that initially ($t = 0$) the mediators were in reduced forms only:

$$[\mathrm{Red}]_{t=0} = [\mathrm{Med}_T] \tag{14}$$

$$[\mathrm{Ox}]_{t=0} = 0 \tag{15}$$

where $[\mathrm{Med}_T]$ is the total concentration of the redox mediators.

At the electrode surface ($x = 0$) for cyclic voltammetry the boundary conditions are:

-the Nernst equilibrium:

$$\frac{[\mathrm{Ox}]_{x=0}}{[\mathrm{Red}]_{x=0}} = \exp\left(\frac{nF(E_i + vt - E^{0\prime})}{RT}\right) \tag{16}$$

-the balance of the molar fluxes of the reduced and oxidized species:

$$D_{app}\frac{\partial[\mathrm{Red}]}{\partial x}\bigg|_{x=0} = -D_{app}\frac{\partial[\mathrm{Ox}]}{\partial x}\bigg|_{x=0} \tag{17}$$

The value of the current density is given at any time by the flux of the oxidized or the reduced species at the electrode surface:

$$J = nFD_{app}\frac{\partial[\mathrm{Red}]}{\partial x}\bigg|_{x=0} = -nFD_{app}\frac{\partial[\mathrm{Ox}]}{\partial x}\bigg|_{x=0} \tag{18}$$

Only the boundary conditions far from the electrode surface differ, depending on the "Nernst diffusion layer" or the "thin layer" hypothesis. The purpose of the next two sub-sections is to assess the extent to which the semi-infinite diffusion and the ideal thin layer analytical solutions may provide a suitable framework to represent electron transfer in EA biofilms.

3.2 Nernst-diffusion layer model and assessment of the semi-infinite diffusion hypothesis

The Nernst-diffusion layer model assumes a diffusion layer of finite thickness (δ_{diff}), beyond which the concentrations of the reduced and oxidized species are uniform (Fig. 1C). Concentration gradients occur only in the diffusion layer located on the electrode surface, while each dissolved species has a uniform and constant concentration in the bulk solution. It is thus tacitly assumed that the production and consumption of redox species during the analysis do not change the concentrations in the bulk. For this assumption be valid, care must be taken to use a small electrode surface area in a large volume of solution. For example, this model is commonly used for rotating disc electrodes, where the value of δ is determined by the speed of rotation of the electrode and the physicochemical properties of the solution.[32] Actually, the Nernst-diffusion layer hypothesis gives a general framework, in which the semi-infinite diffusion hypothesis is a limit case obtained by pushing δ towards infinity. In other words, increasing δ towards very large values allows the conditions of semi-infinite diffusion to be recovered.

When a biofilm is present on the electrode surface, the diffusion layer can be larger than the biofilm thickness. The diffusion layer will approximately be equal to the biofilm thickness in the case of sufficient stirring of the solution or if diffusion rates inside the biofilm are slower than in solution. In other cases the biofilm is a part of a larger diffusion layer. The possible differences of the diffusion rates inside and outside the biofilm would be part of a more sophisticated approach that is not addressed here and do not affect the conclusions drawn here.

According to the Nernst-diffusion layer model, the concentrations at the interface between the diffusion layer and the bulk ($x = \delta$) remain identical to the initial conditions:

$$[\mathrm{Red}]|_{x=\delta} = [\mathrm{Med}_T] \tag{19}$$

$$[\mathrm{Ox}]|_{x=\delta} = 0 \tag{20}$$

The partial derivative eqn (12) and (13) combined with the boundary ($x = 0$ and $x = \delta$) and initial ($t = 0$) conditions give a comprehensive set of equations that can be solved numerically.

Before numerically solving this system, the number of independent parameters to be considered was reduced by switching the equations into dimensionless form. The reference parameters were the diffusion layer thickness δ for distances, the total concentration of the mediator molecules $[\mathrm{Med}_T]$ for concentrations, D_{app}/δ^2 for time, and RT/nF for potential, so that:

$$\overline{x} = \frac{x}{\delta} \tag{21}$$

$$\overline{t} = \frac{D_{app}}{\delta^2}t \tag{22}$$

$$\overline{[\mathrm{Red}]} = \frac{[\mathrm{Red}]}{[\mathrm{Med}_T]}; \overline{[\mathrm{Ox}]} = \frac{[\mathrm{Ox}]}{[\mathrm{Med}_T]} \tag{23}$$

$$\overline{J} = \frac{J}{\frac{nFD_{\mathrm{app}}[\mathrm{Med}_T]}{\delta}} \tag{24}$$

$$\overline{E} = \frac{nF}{RT}E \text{ and } \overline{E_{\mathrm{ini}}} = \frac{nF}{RT}(E_{\mathrm{ini}} - E^{0\prime}) \tag{25}$$

$$\overline{v} = \frac{nF\delta^2}{RTD_{\mathrm{app}}}v \tag{26}$$

The set of partial derivatives to be solved became:

$$\frac{\partial\overline{[\mathrm{Red}]}}{\partial\overline{t}} = \frac{\partial^2\overline{[\mathrm{Red}]}}{\partial\overline{x}^2} \tag{27}$$

$$\frac{\partial\overline{[\mathrm{Ox}]}}{\partial\overline{t}} = \frac{\partial^2\overline{[\mathrm{Ox}]}}{\partial\overline{x}^2} \tag{28}$$

the initial conditions:

$$\overline{[\mathrm{Red}]}|_{\overline{t}=0} = 0 \tag{29}$$

$$\overline{[\mathrm{Ox}]}|_{\overline{t}=0} = 0 \tag{30}$$

the boundary conditions at the electrode surface ($\overline{x} = 0$):

$$\frac{\overline{[\mathrm{Ox}]}_{\overline{x}=0}}{\overline{[\mathrm{Red}]}_{\overline{x}=0}} = \exp(\overline{E_{\mathrm{ini}}} + \overline{v}\overline{t}) \tag{31}$$

$$\left.\frac{\partial\overline{[\mathrm{Red}]}}{\partial\overline{x}}\right|_{\overline{x}=0} = -\left.\frac{\partial\overline{[\mathrm{Ox}]}}{\partial\overline{x}}\right|_{\overline{x}=0} \tag{32}$$

$$\overline{J} = \left.\frac{\partial\overline{[\mathrm{Red}]}}{\partial\overline{x}}\right|_{\overline{x}=0} \tag{33}$$

and at the diffusion layer/bulk interface ($\overline{x} = 1$):

$$\overline{[\mathrm{Red}]}|_{\overline{x}=1} = 1 \tag{34}$$

$$\overline{[\mathrm{Ox}]}|_{\overline{x}=1} = 0 \tag{35}$$

This set of equations was solved numerically. Obviously, the potential scan rate must start from an initial value $\overline{E_{\mathrm{ini}}}$ consistent with the initial concentration profile (eqn (29) and (30)). Here $\overline{E_{\mathrm{ini}}}$ was equal to -6 (corresponding to E_{ini} of 150 mV smaller than $E^{0\prime}$) to ensure an initial concentration of the reduced form of less than 0.003. The potential was then varied by steps at the scan rate $\bar{v}$ to obtain the variation of the concentration profiles (Fig. 2) and, at each iteration, the current density was calculated through eqn (33). Plotting $\bar{J}$ as a function of $\bar{E}$ gave the CV curves as shown in Fig. 3A. CV curves were plotted in this manner for different values of the potential scan rate ($\bar{v}$) and the $\overline{J_{\mathrm{peak}}}$ value extracted from each CV curve was finally reported as a function of $\bar{v}$ (Fig. 3B).

At the lower potential scan rate values, the model gives the conventional stationary CV curve exhibiting no current peak. In dimensionless values, at the stationary state, the diffusion-limited current $\bar{J}_{\mathrm{lim}}$ is equal to unity, which corresponds to the conventional expression of the diffusion-limited current in the Nernst-diffusion layer hypothesis:

$$J_{\mathrm{lim}} = \frac{nFD_{\mathrm{app}}[\mathrm{Med}_T]}{\delta} \tag{36}$$

The stationary state is ensured for values of the dimensionless scan rate lower than around 5:

$$\overline{v}_{\mathrm{stationary}} \leq 5 \text{ or } v_{\mathrm{stationary}} \leq 5\frac{RTD_{\mathrm{app}}}{nF\delta^2} \tag{37}$$

This indicates that, in order to observe a transient peak, the scan rate must be increased if the apparent diffusion coefficient D_{app} is suspected to be high or the diffusion layer δ suspected to be thin (for example in the case of thin biofilms and efficient stirring and/or high rotating speed of a rotating disk electrode). Taking a diffusion coefficient value of an easily diffusing species (hexacyanoferrate for instance[33]) of 7.6×10^{-10} m^2 s^{-1}, the scan rate required to provoke the transient response is around 40 mV s^{-1} for a 50 μm diffusion layer thickness.

Fig. 3B shows that, as soon as the current peak appeared ($\log(\bar{v}) \geq 0.69$), it varied proportionally to $\bar{v}^{1/2}$ in the whole range of $\bar{v}$ values. The $J_{\mathrm{peak}} \div v^{1/2}$ relationship was consequently valid in all cases and was not linked to the

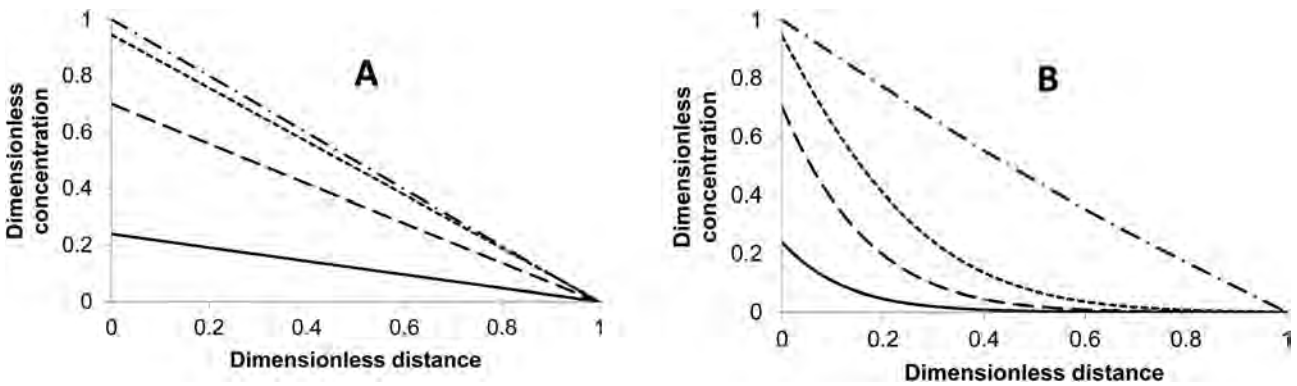

Fig. 2 Nernst diffusion layer hypothesis: dimensionless concentration profiles of the oxidized species ($\overline{[\mathrm{Ox}]}$) in the diffusion layer ($0 < \delta < 1$) at potentials ($\bar{E}$) of -2 (straight line); 0 (dashed line); 2 (dotted line) and 20 (dotted-dashed line); (A) in stationary state at low scan rate ($\bar{v} = 0.1$) all concentration profiles are linear; (B) at transient state at high scan rate ($\bar{v} = 80$).

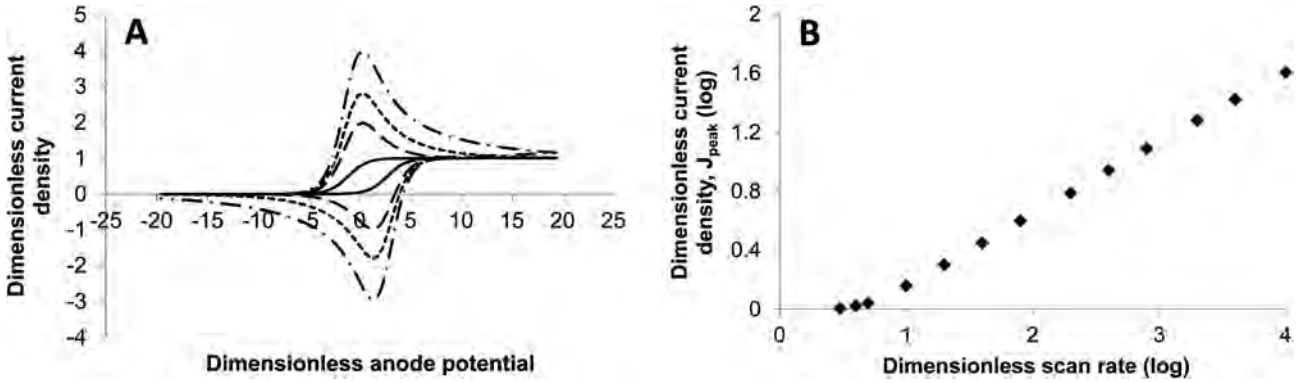

Fig. 3 Nernst diffusion layer hypothesis; (A) cyclic voltammograms at different dimensionless scan rates ($\bar{v}$): 1 (straight line); 20 (dashed line); 40 (dotted line) and 80 (dotted-dashed line); (B) the log–log relationship between the dimensionless current density peak ($\bar{J}_{peak}$) and the dimensionless scan rate ($\bar{v}$).

semi-infinite hypothesis. A finite diffusion layer, whatever its thickness, leads to the same J_{peak} *vs.* v^{α} relationship with the α exponent equal to 0.5. This relationship was established through the formal hypothesis of semi-infinite diffusion, which is quite far from real experimental conditions but, fortunately, remains valid when the biofilm is treated as a finite diffusion layer. The first part of the question of Section 2 can now be answered: the supposed semi-infinity of space in front of the electrode surface does not affect the validity of the $J_{peak} \div v^{1/2}$ relationship in the case of freely-diffusing mediators.

Nevertheless, the finite diffusion layer gave a distant representation of the phenomena that occur in the most EA biofilms. Actually, the whole solution contained in the reactor is assumed to contain the redox mediators and the biofilm is taken to act only as a passive diffusion layer. This representation can be justified for experimental systems in which the EA biofilm produces a diffusible redox mediator that accumulates in the bulk solution or

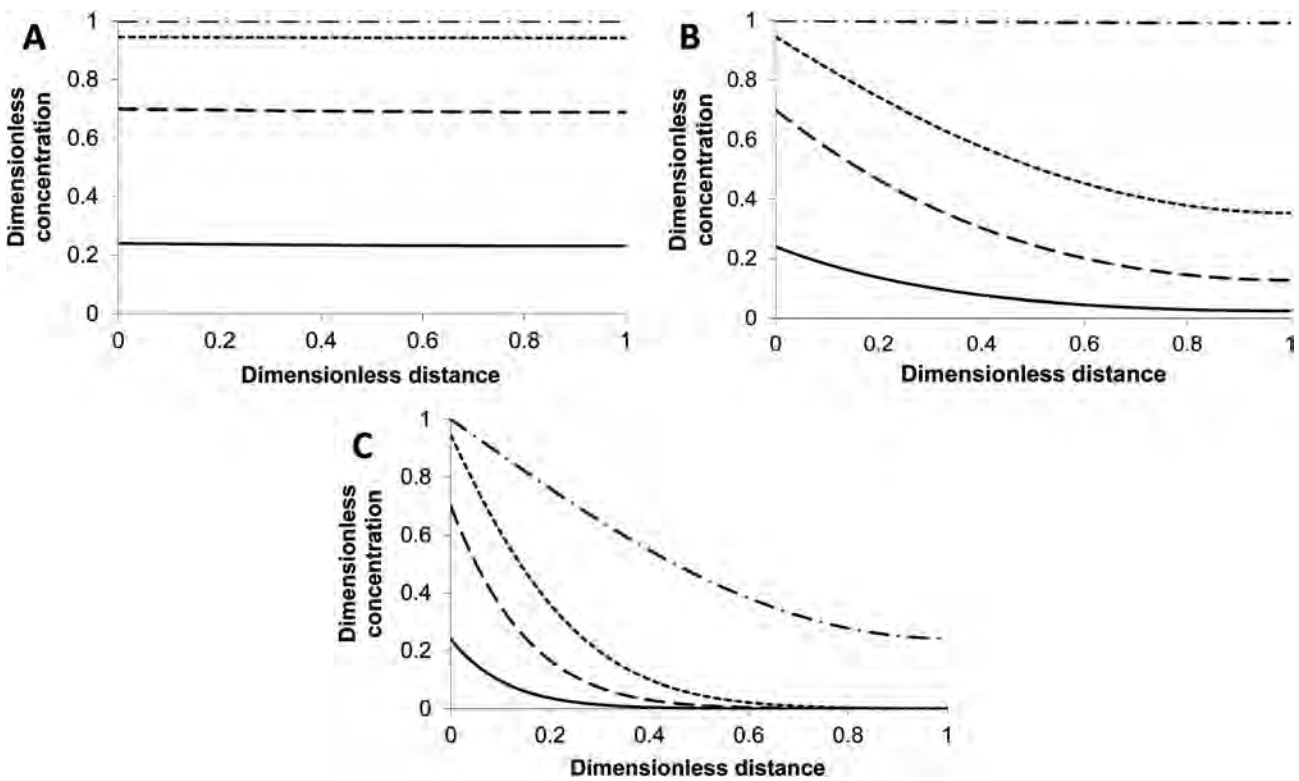

Fig. 4 Thin layer hypothesis: dimensionless concentration profiles of the oxidized species ($[\overline{Ox}]$) in the diffusion layer ($0 < \delta < 1$) at potentials ($\bar{E}$) of -2 (straight line); 0 (dashed line); 2 (dotted line) and 20 (dotted-dashed line); (A) in stationary state at low scan rate ($\bar{v} = 0.1$) the concentration gradients in the layer can be neglected, the conditions of "ideal thin layer" are valid in this case; (B) at $\bar{v} = 10$ concentration gradients occur inside the layer; (C) at $\bar{v} = 100$ even at the end of the potential scan, the concentration is not uniform in the layer; in (B) and (C) cases, concentration gradients cannot be neglected, the ideal thin layer hypothesis is consequently no longer valid.

for artificial mediators that are added into solution. Nevertheless, this approach is less relevant for EA biofilms that use the electron transport pathways that are confined in the biofilm matrix. The $J_{peak} \div v^{1/2}$ relationship was consequently established in a theoretical framework far from conditions relating to a lot of EA biofilms, for which redox mediators and electron transport tools are assumed to be retained inside the biofilm matrix.

3.3 Diffusion inside a thin layer

The ideal thin layer hypothesis used in Section 2 is strictly valid only in very thin cells, *i.e.* with a thickness smaller than that of the diffusion layer induced by the variation of the electrode potential.[34] In fact, concentration gradients can no longer be neglected as soon as the scan rate increases.[35,36] The actual phenomena must then be modelled through a (non-ideal) thin layer model, which includes diffusion between the electrode surface at $x = 0$ and a hermetic frontier at $x = \delta$. The redox species entrapped inside the layer are not able to move outside it (Fig. 1D).

This model is a perfect fit for the case of an EA biofilm of thickness δ, in which the compounds that contribute to the electron transport are retained. The apparent diffusion of the electron inside a network of immobilized cytochromes is an obvious example, but the model can also be valid with diffusible redox mediators. Producing extracellular redox compounds requires high energy expenditure from the microbial cell. Any leakage of the redox mediator from the biofilm is a drastic energy loss for the cells and may call biofilm survival into question. EA biofilms have been shown to develop sophisticated strategies to confine the extracellular diffusible mediators inside the biofilm volume and avoid leakage to the solution.[37] The thin layer model gives consequently a very appropriate theoretical framework for approaching the electrochemistry of biofilms.

The model is based on the same set of partial derivative equations (eqn (12) and (13)) with the same initial conditions (eqn (14) and (15)) and the same boundary conditions at the electrode surface (eqn (16)–(18)) as in the previous sub-section, but with changed boundary conditions at $x = \delta$ to express the confinement of the redox species:

$$D_{app} \left.\frac{\partial[\mathrm{Red}]}{\partial x}\right|_{x=\delta} = 0 \tag{38}$$

$$D_{app} \left.\frac{\partial[\mathrm{Ox}]}{\partial x}\right|_{x=\delta} = 0 \tag{39}$$

or, in dimensionless form:

$$\left.\frac{\partial[\overline{\mathrm{Red}}]}{\partial \bar{x}}\right|_{\bar{x}=1} = 0 \tag{40}$$

$$\left.\frac{\partial[\overline{\mathrm{Ox}}]}{\partial \bar{x}}\right|_{\bar{x}=1} = 0 \tag{41}$$

The numerical process conducted as previously led to the concentration profiles shown in Fig. 4 and the CV curves for different scan rates in Fig. 5. At low scan rate, the CV curves calculated with the thin layer hypothesis do not show stationary behaviour as was the case for the diffusion layer model (Fig. 3A). There is no diffusion-limited current but, in contrast, a current peak always occurs with the current falling to zero at high potentials. The different CV patterns given by the Nernst diffusion layer model (Fig. 3A) and the thin layer model (Fig. 5A) are consistent with the basic hypotheses. In the Nernst diffusion layer model, the diffusion layer is continuously provided with redox species from the bulk solution and the balance between the consumption of reduced species and their transfer from the bulk leads to the stationary state. In contrast, the amount of available redox compound is limited in the thin layer model and the current peak is due to its depletion up to complete consumption.

At low potential scan rates, the current peak varies with the scan rate according to eqn (11), which, in dimensionless form, gives:

$$\overline{J}_{peak} = \frac{\overline{v}}{4} \tag{42}$$

so that:

$$\log(\bar{J}_{peak}) = \log(\bar{v}) - 0.6 \tag{43}$$

which fits the linear part of the curve plotted in Fig. 5B perfectly for scan rates $\bar{v}$ smaller than 1 ($\log(\bar{v}) \leq 0$). The thin layer

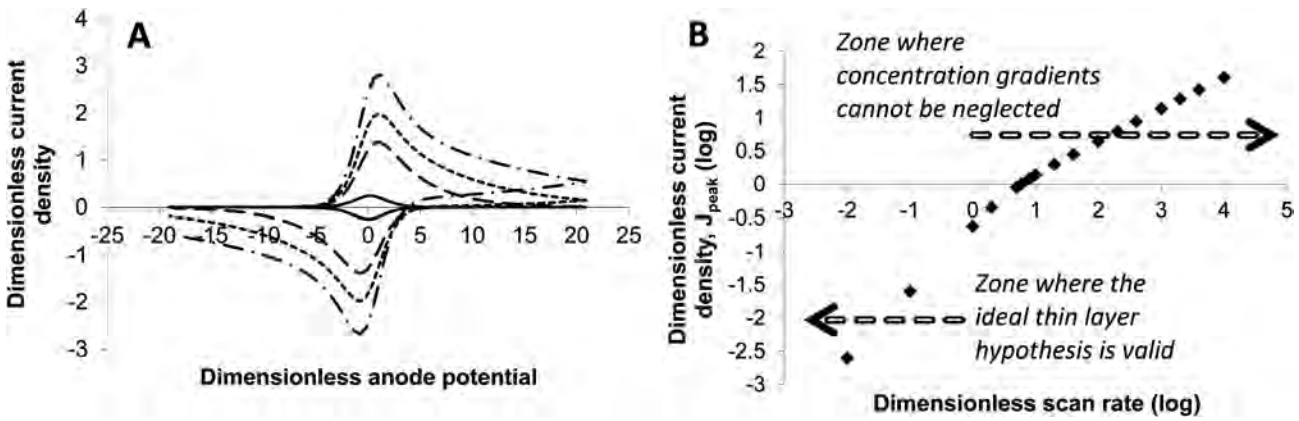

Fig. 5 Thin layer hypothesis; (A) cyclic voltammograms at different values of the dimensionless scan rate ($\bar{v}$): 1 (straight line); 10 (dashed line); 20 (dotted line) and 40 (dotted-dashed line) (B) log–log relationship between the dimensionless current density peak ($\bar{J}_{peak}$) and the dimensionless scan rate ($\bar{v}$).

hypothesis and the $J_{peak} \div v^1$ relationship are consequently valid for scan rates $\bar{v}$ smaller than 1. In this case, the layer is thin enough for concentration gradients to be neglected inside it (Fig. 4A).

When the value of $\bar{v}$ increases above 1, the system deviates from the ideal thin layer behaviour because concentration gradients can no longer be neglected in the cell (Fig. 4B). The exponent α of the J_{peak} *vs.* v^α relationship decreases from 1 towards 0.5. Above a dimensionless scan rate of approximately 20, the current peak varies as $\bar{v}^{1/2}$. High values of the dimensionless scan rate are obtained at high values of the scan rate coupled with high values of the layer thickness and small diffusion coefficients. Under such conditions, varying the potential of the electrode disturbs the concentration profiles only close to the electrode surface. Because of the large thickness and/or the low diffusion coefficient and/or the rapidity of the potential scan, the concentration profiles are not affected by the layer limit at $x = \delta$ (Fig. 4C). The boundary condition at $x = \delta$ no longer matters and the system behaves as in the semi-infinite diffusion hypothesis.

The second part of the question of Section 2 can now be answered: an EA biofilm can be modelled by the ideal thin layer hypothesis only if its thickness is small enough to ensure a dimensionless scan rate lower than unity. Above this value, its behaviour departs drastically from the J_{peak} *vs.* v^1 relationship.

3.4 Conclusions relating to electron transport in EA biofilms extracted from non-turnover CV

In conclusion to Section 3, a few simple theoretical rules can be stated. When electron transport is achieved *via* redox species that accumulate in the bulk solution and diffuse freely through the biofilm, the $J_{peak} \div v^\alpha$ relationship has an α exponent equal to 0.5 over the whole scan rate range. On the CV curves, this case can be recognized by the occurrence of an unchanged stationary CV curve at low scan rates ($\bar{v} < 5$), with a diffusion-limited current equal to unity in dimensionless form ($\bar{J}_{lim} = 1$, eqn (36)). When the scan rate increases ($\bar{v} > 5$) a transient peak appears, superimposed on the stationary current, but the diffusion-limited current remains unchanged at the highest potentials.

In contrast, when electron transport is controlled by a diffusion-like process that is confined inside the biofilm, the CV curves exhibit a peak current at any scan rate, even the lowest. This case does not include a stationary current because the quantity of redox compound is limited by the small volume of the biofilm and there is no supply from outside the biofilm. At low scan rates, the current falls to zero after the peak whereas, at high scan rates, the current after the peak increases with the scan rate. At low scan rates ($\bar{v} < 1$) the $J_{peak} \div v^\alpha$ relationship leads to $\alpha = 1$; at high scan rates ($\bar{v} > 20$) it gives $\alpha = 0.5$. In the intermediate range ($1 < \bar{v} < 20$) the α exponent moves from 1 to 0.5. This intermediate range may explain the variety of α values that have been reported in the literature.[18,21] This study shows that it is not useful to contemplate complex unidentified mechanisms to explain α values between 0.5 and 1, but the simple response of an EA biofilm that obeys a thin layer model can support a large range of α values.

Experimentally, it is often difficult to work on a sufficiently large range of scan rates to differentiate the two cases by stating whether α is constant or varies from 1 to 0.5. Most often, because of the long time required for low scan rate CVs or the occurrence of capacitive currents at high scan rates, the J_{peak} *vs.* v^α relationship can be recorded experimentally only in a fairly narrow range of scan rates. Consequently, the experimental data generally give access to only a narrow part of the J_{peak} *vs.* v^α relationship. Under such conditions, any value of α between 1 and 0.5 may be found if CVs are recorded in the $1 < \bar{v} < 20$ range or in a restricted zone that includes this range.

Nevertheless, a few sound conclusions can be extracted from the experimental data. When the J_{peak} *vs.* v^α relationship leads to α equal to 1, it can be concluded that electron transport is achieved *via* confined redox compounds. This conclusion is valid for any process that can be modelled by a diffusion equation confined in the biofilm space, for example, electron hopping between immobilized redox compounds or mass transfer of diffusible mediators that remain entrapped inside the biofilm. So it must be kept in mind that α equal to 1 does not mean that electron transport is necessarily achieved by immobilized molecules (a chain of immobilized cytochromes for example) as α equal to 1 can also be perfectly applicable to the case of diffusible mediators that are retained inside the biofilm (by hydrophilic/phobic interactions for example[37]). α equal to 1 also indicates that the CV curves were recorded at low dimensionless scan rates ($\bar{v} < 1$), meaning that thin biofilms and high apparent diffusion coefficient can be suspected (eqn (26)). This case should consequently correspond to thin, efficient EA biofilms. The variation of the current peak as a function of the scan rate extracted from eqn (42):

$$J_{peak} = \frac{n^2 F^2 [\mathrm{Med}_T] \delta}{4RT} v \qquad (44)$$

can be used to estimate the concentration of the mediator compounds in the biofilm $[\mathrm{Med}_T]$ if the biofilm thickness (δ) can be determined by another method, microscopy for instance, and assuming that electrons are transported *via* mono-electronic reactions ($n = 1$) as is the case for most redox mediators, cytochromes in particular.

An experimental value of α of 0.5 can correspond to two different electron transport mechanisms: either freely diffusing redox mediators accumulated in solution or confined redox compounds. In this case, the sole variation of J_{peak} *vs.* v is not sufficient to conclude on the nature of the electron transport mechanism, but the form of the CV curves may help. The occurrence of a diffusion-limited current should indicate a freely diffusing mediator but it might be difficult to differentiate a diffusion-limited current from the limiting catalytic current described in the next section (see Section 4). Experimentally, the best way to differentiate a freely diffusing mediator process from a confined process is to repeat the CV recording in a fresh solution. Placing the electrode in fresh solution, in which no mediator has accumulated, should make the CV currents vanish in the first case, while it would not change CV curves in the second case. Mixed cases should also be identified in this way and the proportion of each mechanism could be estimated. If the

mechanism is supported by a confined process, it can be concluded that CV curves were recorded at high dimensionless scan rates ($\bar{\nu} > 20$), meaning that thick biofilms and low apparent diffusion coefficient can be suspected. This case should consequently correspond to thick, poorly efficient EA biofilms.

4. Coupled electron transport and metabolic reaction rate in the thin layer model: catalytic CV

4.1 General equations for coupled electron transport and metabolic reaction

Let us consider the most common case of a bioanode oxidizing acetate:

$$CH_3COO^- + 4H_2O \rightarrow 2\,HCO_3^- + 9H^+ + 8e^- \quad (45)$$

The bacterial cells oxidize acetate and transfer the electrons to the biofilm redox compounds (diffusive species and/or first link of a chain of immobilized redox molecules), according to a reaction schematized as:

$$Mic_{red} + 8Ox \xrightarrow{k} Mic_{ox} + 8Red \quad (46)$$

where Mic_{red} and Mic_{ox} represent the microbial cells before and after releasing the electrons. As commonly done,[14,15] it is postulated that the 8 electrons produced per acetate molecule are transferred to 8 mediator molecules *via* mono-electronic bimolecular reactions, the rate of which is:

$$Rate = k\,[Mic_{red}]\,[Ox] \quad (47)$$

The set of partial derivative equations that represents the coupled electron transport/reaction in an EA biofilm is thus:

$$\frac{\partial[Red]}{\partial t} = D_{app}\frac{\partial^2[Red]}{\partial x^2} + 8Rate \quad (48)$$

$$\frac{\partial[Ox]}{\partial t} = D_{app}\frac{\partial^2[Ox]}{\partial x^2} - 8Rate \quad (49)$$

completed with the equation relative to acetate:

$$\frac{\partial[Ac]}{\partial t} = D_{Ac}\frac{\partial^2[Ac]}{\partial x^2} - Rate \quad (50)$$

where [Ac] is the concentration of acetate and D_{Ac} is its diffusion coefficient.

The metabolic reaction rate was modelled using the theoretical scheme that Lovley, Tender and co-workers derived for EA biofilms[14,15] from previous theoretical studies devoted to enzyme-modified electrodes.[38,39] In similarity with enzymatic mechanisms, the acetate uptake and oxidation by the bacterial cells is assumed to obey Michaelis–Menten kinetics. Acetate uptake is taken into account by an equilibrated reaction, with the equilibrium constant K_M that expresses the affinity of the microorganism for acetate:

$$Mic_{ox} + Ac^- \xleftrightarrow{K_M} Mic_{ox} - Ac^- \quad (51)$$

where Mic_{ox}–Ac represents an intermediate form by similarity to the enzyme–substrate complex in enzyme kinetics. Acetate is then oxidized through the metabolic pathway with an overall rate constant k_{cat}:

$$Mic_{ox} - Ac^- + 4H_2O \xrightarrow{k_{cat}} Mic_{red} + 2HCO_3^- + 9H^+ + 8e^- \quad (52)$$

The stationary-state hypothesis applied to the Mic_{red} species:[40]

$$k_{cat}\,[Mic_{ox}\text{–}Ac^-] - k\,[Mic_{red}]\,[Ox] = 0 \quad (53)$$

combined with conservation of the different microbial forms:

$$[Mic_T] = [Mic_{ox}] + [Mic_{red}] + [Mic_{ox}\text{–}Ac^-] \quad (54)$$

where $[Mic_T]$ is the total concentration of microbial cells in the biofilm, leads to the concentration of the reduced form of the microbial cells:

$$[Mic_{red}] = \frac{k_{cat}}{k[Ox]}\frac{[Mic_T]}{1 + \frac{k_{cat}}{k[Ox]} + \frac{K_M}{[Ac]}} \quad (55)$$

and finally to the developed expression for the rate:

$$Rate = k_{cat}\frac{[Mic_T]}{1 + \frac{k_{cat}}{k[Ox]} + \frac{K_M}{[Ac]}} \quad (56)$$

that can be used to solve the set of partial derivative eqn (48) and (50).

The initial conditions are unchanged (eqn (14) and (15)) for the mediator species and a uniform concentration of acetate is assumed:

$$[Ac]_{t=0} = [Ac]^B \quad (57)$$

where $[Ac]^B$ is the concentration of acetate in the solution bulk. At the electrode surface, the boundary conditions were also unchanged for the mediator, expressing the Nernst equilibrium and the flux balance between the oxidized and reduced species (eqn (16) and (17)). Acetate does not react at the electrode surface; its flux is consequently zero:

$$D_{app}\frac{\partial[Ac]}{\partial x}\bigg|_{x=0} = 0 \quad (58)$$

The thin layer model was used here because confinement of the electron transport tools inside the biofilm is a more likely situation for EA biofilms than diffusion of a soluble mediator previously accumulated in the bulk solution. At the biofilm frontier ($x = \delta$), the boundary conditions thus express the confinement of the redox species (eqn (38) and (39)) while it was assumed that acetate was not affected by the mass transfer limitation out of the biofilm:

$$[Ac]_{x=\delta} = [Ac]^B \quad (59)$$

4.2 Simplification to first-order metabolic kinetics

To make a first foray into the behaviour of the system, some usual hypotheses can be made to simplify the system:[14,15]

- The acetate concentration is high enough not to be rate-limiting. It has generally been observed that, above values of

around 10 mM, the acetate concentration no longer affects the current provided by microbial anodes. In this case, $[Ac] \gg K_M$ and the ratio $\frac{K_M}{[Ac]}$ can be neglected with respect to unity in the denominator;

- The oxidation metabolic reactions that produce electrons are faster than the final extraction of the electron from the cell *via* the reduction of outer membrane mediators, meaning that $k_{cat} \gg k[Ox]$ and the ratio $\frac{k_{cat}}{k[Ox]}$ becomes predominant in the denominator, which leads to:

$$\text{Rate} = k\,[\text{Mic}_T]\,[\text{Ox}] \tag{60}$$

Actually, these two hypotheses are equivalent to assuming that the acetate concentration is high enough and the metabolic rate fast enough to ensure constant and complete reduction of the microbial cells at any time and throughout the biofilm ($[\text{Mic}_{red}] = [\text{Mic}]$). This is the reason why eqn (50) relating to acetate transport is no longer useful in the framework of this hypothesis set.

The number of parameters to be considered is reduced by switching the equations to dimensionless form. The reference parameters are the same as described above (eqn (21)–(26)) and the initial and boundary conditions are identical to the previous ones (eqn (29)–(32), (40) and (41)). The set of differential equations to be solved becomes:

$$\frac{\partial\overline{[\text{Red}]}}{\partial\bar{t}} = \frac{\partial^2\overline{[\text{Red}]}}{\partial\bar{x}^2} + 8\text{Da}\overline{[\text{Ox}]} \tag{61}$$

$$\frac{\partial\overline{[\text{Ox}]}}{\partial\bar{t}} = \frac{\partial^2\overline{[\text{Ox}]}}{\partial\bar{x}^2} - 8\text{Da}\overline{[\text{Ox}]} \tag{62}$$

where the dimensionless Damköhler number appears:

$$\text{Da} = \frac{k[\text{Mic}_T]\delta^2}{D_{app}} \tag{63}$$

Here the Da number is related to the extracellular electron transfer from the microbial cells to the redox network of the biofilm. In the framework of the simplified approach, the other steps of the reaction chain were assumed to be faster and not to affect the whole kinetics. Da thus expresses the ratio of the maximum reaction rate of electron extraction from the cells ($k[\text{Mic}_T][\text{Med}_T]\delta$)) over the maximal rate of electron transport through the redox biofilm network $\left(\frac{D_{app}[\text{Med}_T]}{\delta}\right)$.

The CV curves (Fig. 6) show that stationary curves are obtained at low scan rates. The stationary state is reached inside the thin layer when the electrochemical consumption of the redox species is balanced by its continuous regeneration by the metabolic reaction. The maximum current density plateau corresponds to the limiting catalytic current density controlled by the rate of the metabolic reaction. When the Damköhler number increases, the stationary state is maintained up to

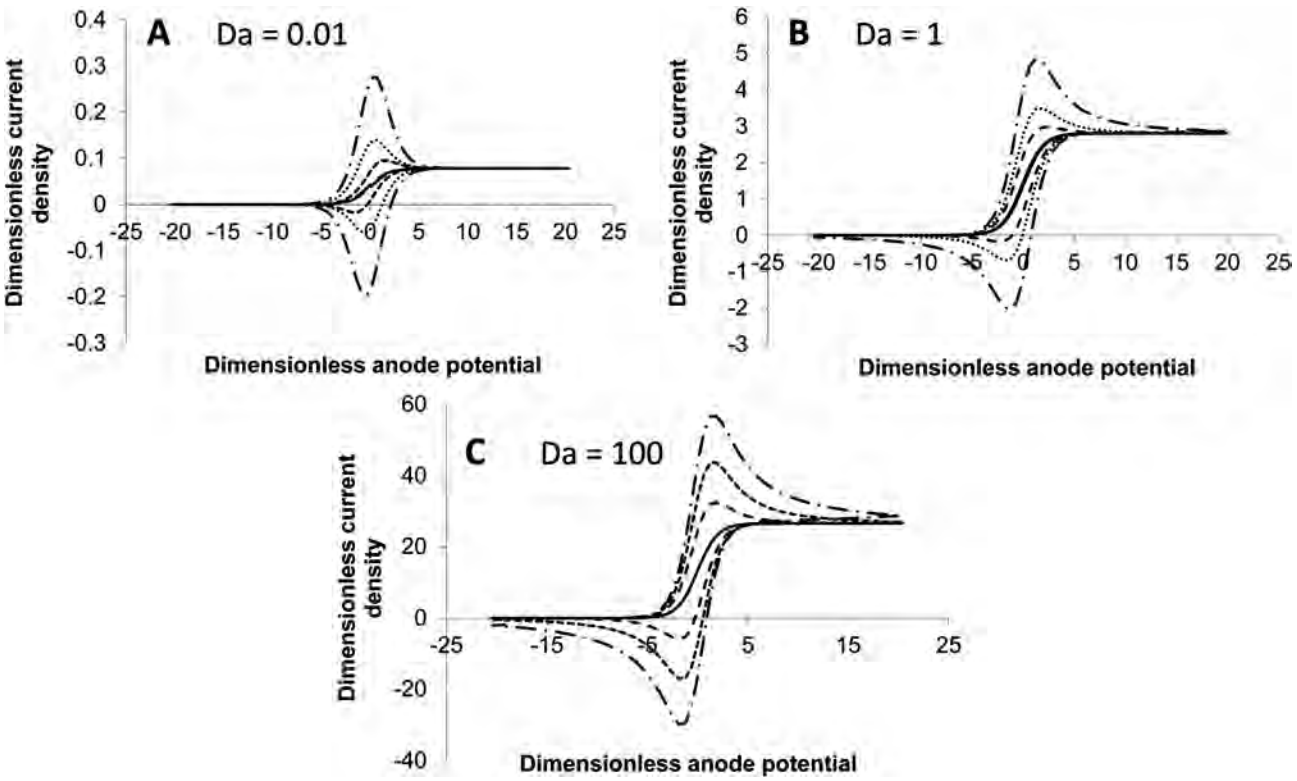

Fig. 6 Electron transport coupled with a first-order metabolic reaction treated in the framework of the thin layer hypothesis: cyclic voltammograms obtained for various Damköhler numbers (Da) at different scan rates ($\bar{v}$); (A) Da = 0.01 $\bar{v}$ = 0.01 (straight line); 0.2 (dashed line); 0.4 (dotted line) and 1 (dotted-dashed line); (B) Da = 1 $\bar{v}$ = 1 (straight line); 20 (dashed line); 40 (dotted line) and 100 (dotted-dashed line); C. Da = 100 $\bar{v}$ = 1 (straight line); 4000 (dashed line); 10 000 (dotted line); 20 000 (dotted-dashed line).

higher scan rates and the value of the maximum current increases with the Da number.

The value of the limiting catalytic current density (J_{lim}) can be calculated analytically. At stationary state, eqn (62) becomes:

$$0 = \frac{d^2[\overline{Ox}]}{d\bar{x}^2} - 8Da[\overline{Ox}] \quad (64)$$

The boundary condition at $\bar{x} = 1$ remains unchanged (eqn (41)). The limiting catalytic current corresponds to the maximum electrochemical rate, *i.e.* a complete oxidation of the redox species at the electrode surface:

$$[\overline{Ox}]|_{\bar{x}=0} = 1 \quad (65)$$

This set of equations is solved to:

$$[\overline{Ox}] = -\frac{sh\sqrt{8Da}}{ch\sqrt{8Da}} sh\bar{x}\sqrt{8Da} - ch\bar{x}\sqrt{8Da} \quad (66)$$

so that:

$$\overline{J_{lim}} = \sqrt{8Da}th\sqrt{8Da} \quad (67)$$

which can be simplified for Da greater than around 0.5 to:

$$\overline{J_{lim}} = \sqrt{8Da} \quad (68)$$

and confirms that the limiting catalytic current density increases with Da.

For each Da value, the $\bar{J}_{peak}$ *vs.* $\bar{v}$ curve has a different shape (Fig. 7 and 8). For low values of Da (Da $\leq$ 0.01) the curves are close to the purely diffusive thin layer case (Fig. 5B) with the first part (low $\bar{v}$) corresponding to $\alpha = 1$ and the second part (high $\bar{v}$) giving $\alpha = 0.5$. The presence of the metabolic reaction affects only the low scan rate part of the curve due to the apparition of the stationary state. At low scan rate, the stationary state makes the current peak disappear on the CV curves, and it is consequently no longer possible to plot the first part of the $\bar{J}_{peak}$ *vs.* $\bar{v}$ curve. As suspected (see Section 3.4), slow metabolic reactions (Da < 0.01) do not markedly disturb the CV curves; they only introduce a stationary state at very low scan rates.

For intermediate values of Da (0.01 < Da < 1) the first part of the $\bar{J}_{peak}$ *vs.* $\bar{v}$ curves, which corresponds to $\alpha = 1$, totally disappears. The $\bar{J}_{peak}$ *vs.* $\bar{v}$ curves are thus only made up of the upper part ($\alpha = 0.5$) whose base is truncated by the stationary state. Finally, for high Da values (Da $\geq$ 1) the presence of the metabolic reaction strongly modifies the whole $\bar{J}_{peak}$ *vs.* $\bar{v}$ curves, which are no longer linear. There is a subjective element in the extraction of an α value here but, roughly speaking, it can be stated that increasing Da makes α to decrease.

When Da increases, the $\bar{J}_{peak}$ *vs.* $\bar{v}$ curves are shifted towards higher values of $\bar{v}$ because the scan rate up to which the stationary state is maintained increases. Actually, when the metabolic reaction rate increased, the stationary state was maintained for increasingly higher values of the potential scan rate. It was consequently necessary to use increasingly higher scan rates to observe a current peak on the CV curves. The theoretical model thus fully explains recent experimental results, which exhibit CV curves that do not change and remain identical to the stationary curves when the scan rate increases from 1 to values as high as 100 mV s^{-1}.[41] The model shows that CV curves remaining in the stationary phase even at high scan rates are the mark of the presence of a metabolic reaction coupled with the electron transport process. Furthermore, the model indicates that the higher the Da number is, the longer the steady state is maintained up to high $\bar{v}$. A glance at the $\bar{v}$ and Da expressions (eqn (26) and (63), respectively) indicates that the steady state maintained up to high scan rates corresponds

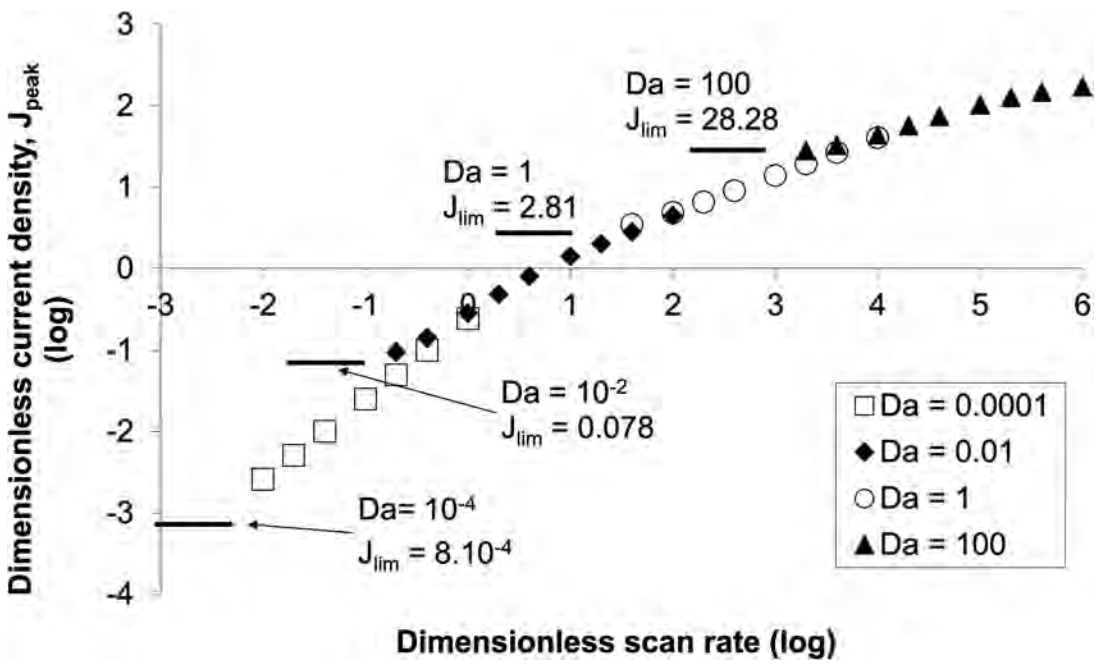

Fig. 7 Electron transport coupled with a first-order metabolic reaction treated in the framework of the thin layer hypothesis: the log–log relationship between the dimensionless current density peak ($\bar{J}_{peak}$) and the dimensionless scan rate ($\bar{v}$).

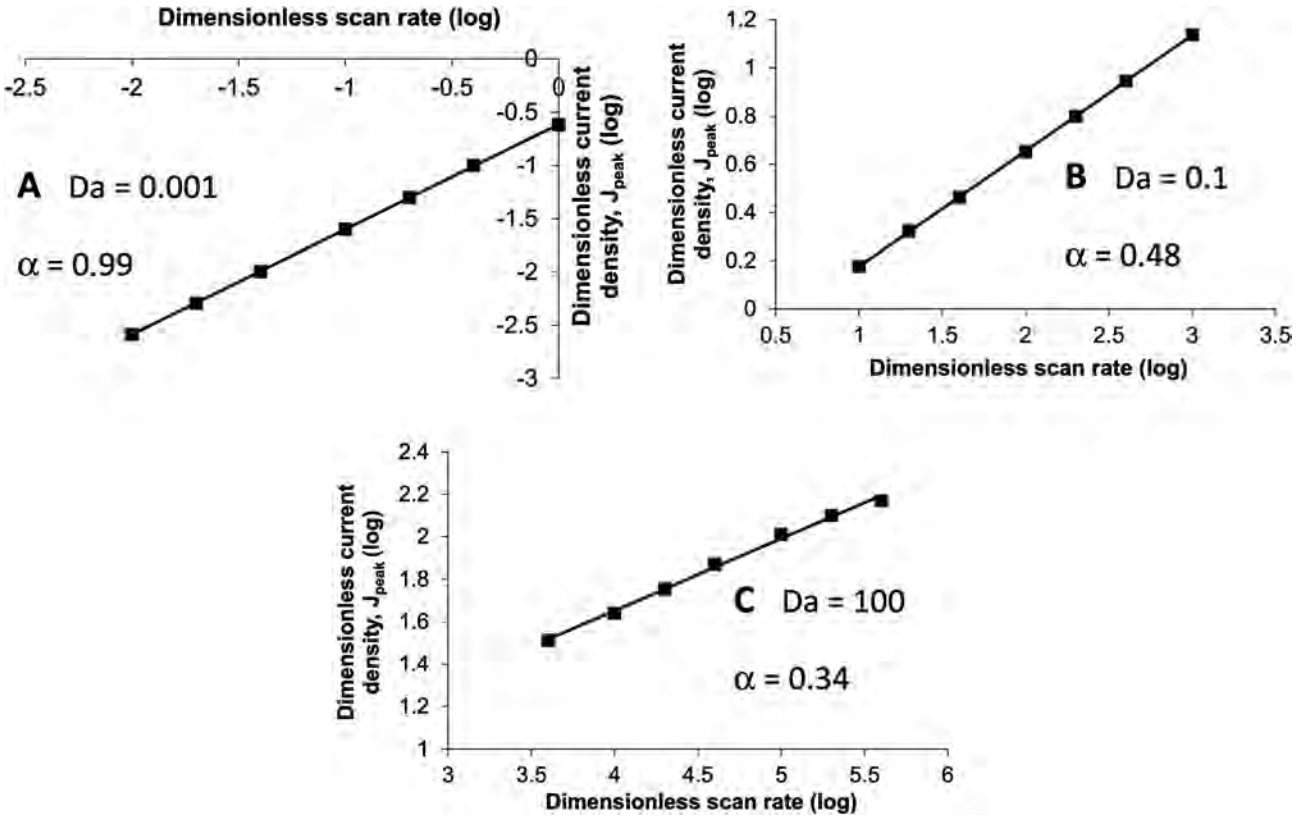

Fig. 8 Electron transport coupled with a first-order metabolic reaction treated in framework of the thin layer hypothesis: log–log relationship between the dimensionless current density peak ($\bar{J}_{peak}$) and the dimensionless scan rate ($\bar{v}$); (A) Da = 0.001, (B) Da = 0.1 and (C) Da = 100.

to high values of k and/or low values of D_{app} and/or high values of δ, *i.e.* fast metabolic reaction coupled with slow electron transport in thick biofilms.

The general trends of the $\bar{J}_{peak}$ *vs.* $\bar{v}$ curves are reported in Table 1 using three characteristics:

-the limiting catalytic current density $\bar{J}_{lim}$, which is the maximum value of the current density obtained at stationary state (eqn (67) or (68)): current peaks are always greater than this minimum threshold value because the transient phenomenon superimposed on the stationary current;

-the scan rate threshold $\bar{v}_{threshold}$ above which the current peak appears on the CV curves. This is the threshold above which the stationary state shifts to the transient state. This value was determined roughly by plotting the CV curves for increasing values of $\bar{v}$ and observing the value at which the peak started to appear;

-the average value of α considering the whole $\log(\bar{J}_{peak})$ *vs.* $\log(\bar{v})$ curve as linear. The hypothesis of linearity of the whole curve is less and less valid for increasing values of Da.

4.3 Conclusions relating to electron transport coupled with metabolic kinetics in EA biofilms (catalytic CV)

Coupling the metabolic reaction with electron transport showed that a large variety of α values can be obtained from the experimental analysis of the J_{peak} *vs.* v curves, even values smaller than 0.5, which was not the case when only electron transport was considered (non-turnover CV). The different α values reported in the literature so far can thus be fully explained by the present theoretical approach. Values of α from 0.34 to 1 can be obtained with EA biofilms in which a diffusion-like electron transport is coupled with a metabolic reaction. It

Table 1 Characteristics of the $\bar{J}$ *vs.* $\bar{v}\alpha$ curves for different values of the Damköhler number (Da): $\bar{J}_{lim}$ limiting catalytic current density; $\bar{v}_{threshold}$ scan rate threshold above which the current peak appeared on the CV curves; average value of α extracted by considering the whole curve as linear

Damköhler number	1×10^{-4}	1×10^{-3}	5×10^{-3}	0.01	0.1	1	10	100
$\overline{J_{lim}}$	1×10^{-4}	1×10^{-3}	5×10^{-3}	7.8×10^{-2}	0.64	2.81	8.79	26.54
$\log(\overline{J_{lim}})$	−4	−3	−2.3	−1.11	−0.19	0.45	0.94	1.42
$\overline{v_{threshold}}$	0.004	0.02	0.1	0.2	2	40	200	2000
α	0.99	0.92	0.66	0.5	0.48	0.47	0.43	0.35

should be noted that the lowest value of α obtained here, of 0.34, was not the theoretical lowest limit; smaller values could be reached with higher Da.

Values of α around unity indicate an electron transfer system confined in the EA biofilm without a significant effect of the metabolic reaction (Da < 0.01). The electron transfer rate is faster than the metabolic reaction. When the metabolic reaction has a more marked effect, the α exponent decreases from 1 to 0.5 with intermediate Da values (0.01 < Da < 1). Values of α smaller than 0.5 indicate the occurrence of a fast metabolic reaction (Da > 1). In this case, the limiting catalytic current can be used to extract the Da value (eqn (68)). The general trend is that the α exponent decreases when the effect of the metabolic reaction increases.

Finally, it should be noted that a range of scan rates as large as possible must obviously be investigated. Nevertheless, practically, an optimum must be found between the number of CVs that can be performed and the possible degradation of the biofilm by too many successive CV recordings. Implementing several bio-electrodes in parallel that exhibit identical electrochemical characteristics should be a relevant experimental strategy. The presence of capacitive currents, which are directly proportional to the potential scan rate, must also not be forgotten. They must be removed before interpreting the data. Nevertheless, the difficulty of assessing them accurately generally becomes a severe limit at high scan rates.

4.4 Resolution with the complete form of the kinetic term

The set of equations (48) and (50) with the non-simplified expression of the kinetics (eqn (55)) gave, in dimensionless form:

$$\frac{\partial\overline{[\mathrm{Red}]}}{\partial\bar{t}} = \frac{\partial^2\overline{[\mathrm{Red}]}}{\partial\bar{x}^2} + 8\mathrm{Da}'\frac{1}{1+\dfrac{\bar{k}}{\overline{[\mathrm{Ox}]}}+\dfrac{\overline{K_\mathrm{M}}}{\overline{[\mathrm{Ac}]}}} \tag{69}$$

$$\frac{\partial\overline{[\mathrm{Ox}]}}{\partial\bar{t}} = \frac{\partial^2\overline{[\mathrm{Ox}]}}{\partial\bar{x}^2} - 8\mathrm{Da}'\frac{1}{1+\dfrac{\bar{k}}{\overline{[\mathrm{Ox}]}}+\dfrac{\overline{K_\mathrm{M}}}{\overline{[\mathrm{Ac}]}}} \tag{70}$$

$$\frac{\partial\overline{[\mathrm{Ac}]}}{\partial\bar{t}} = \overline{D}_\mathrm{Ac}\frac{\partial^2\overline{[\mathrm{Ac}]}}{\partial\bar{x}^2} - \mathrm{Da}'\frac{1}{1+\dfrac{\bar{k}}{\overline{[\mathrm{Ox}]}}+\dfrac{\overline{K_\mathrm{M}}}{\overline{[\mathrm{Ac}]}}} \tag{71}$$

The initial and boundary conditions for the mediator are unchanged and they become, for acetate:

$$\overline{[\mathrm{Ac}]}|_{\bar{t}=0} = \overline{[\mathrm{Ac}]}^\mathrm{B} \tag{72}$$

$$\left.\frac{\partial\overline{[\mathrm{Ac}]}}{\partial\bar{x}}\right|_{\bar{x}=0} = 0 \tag{73}$$

$$\overline{[\mathrm{Ac}]}|_{\bar{x}=1} = \overline{[\mathrm{Ac}]}^\mathrm{B} \tag{74}$$

Consequently, four supplementary dimensionless parameters appear. A dimensionless kinetic constant:

$$\bar{k} = \frac{k_\mathrm{cat}}{k[\mathrm{Med}_T]} \tag{75}$$

which is the ratio between the maximum rate of the metabolic reaction ($k_\mathrm{cat}[\mathrm{Mic}_T]\delta$) and the maximum rate of electron release by the microbial cells; the dimensionless Michaelis-type constant:

$$\overline{K_\mathrm{M}} = \frac{K_\mathrm{M}}{[\mathrm{Med}_T]} \tag{76}$$

the dimensionless diffusion coefficient of acetate:

$$\overline{D}_\mathrm{Ac} = \frac{D_\mathrm{Ac}}{D_\mathrm{app}} \tag{77}$$

and the dimensionless concentration of acetate in the bulk:

$$\overline{[\mathrm{Ac}]}^\mathrm{B} = \frac{[\mathrm{Ac}]^\mathrm{B}}{[\mathrm{Med}_T]} \tag{78}$$

The Damköhler number becomes:

$$\mathrm{Da}' = \frac{k_\mathrm{cat}[\mathrm{Mic}_T]\delta^2}{D_\mathrm{app}[\mathrm{Med}_T]} \tag{79}$$

which, in this case, is related to the metabolic kinetics. It expresses the ratio of the maximum metabolic reaction rate ($k_\mathrm{cat}[\mathrm{Mic}_T]\delta$) over the maximum electron transport rate in the biofilm network ($\frac{D_\mathrm{app}[\mathrm{Med}_T]}{\delta}$). Da′ can also be written as:

$$\mathrm{Da}' = \mathrm{Da}\bar{k} \tag{80}$$

The set of dimensionless equations involves four independent parameters. It would be too long and not really useful to analyse each of the 81 cases that can be defined based on three levels (small, medium, high) for each parameter. Here, only one case is treated, based on the most likely parameter values for a common acetate-oxidizing bioanode. $\bar{k}$ is taken equal to unity, assuming that the maximum possible rate of the metabolic reaction and the maximum possible rate of electron release from the cells are equal; $\overline{K_\mathrm{M}} = 5$ assumes a high affinity of the cells for the substrate; Di = 76 corresponds to a standard diffusion coefficient (7.6×10^{-10} m^2 s^{-1})[33] over an apparent diffusion coefficient in the biofilm (here 1×10^{-11} m^2 s^{-1}) and the concentration of acetate $\overline{[\mathrm{Ac}]}^\mathrm{B}$ is taken to be equal to 10.

As $\bar{k}$ is taken equal to unity, the expressions of Da and Da′ are identical (eqn (80)). The results of the simplified first-order kinetics and the Michaelis-Menten-type kinetics can consequently be compared for the same value of the Da and Da′ numbers. Here, with Da′ = 1, the CV curves (Fig. 9A) are very close to those obtained with the first-order kinetics. The value of α extracted from the J_peak *vs.* v^α curves is around 0.47, while it is 0.48 for the first-order kinetics (Table 1). Moreover, the concentration profiles of acetate (Fig. 9B) show very little variation of the acetate concentration in the biofilm, confirming that its mass transport is not limiting and can be neglected. It can be concluded that for the most conventional parameter values, a first-order kinetics law with respect to the oxidized mediator species gives a satisfactory approach to the coupled metabolic reaction/electron transport process in a microbial bioanode.

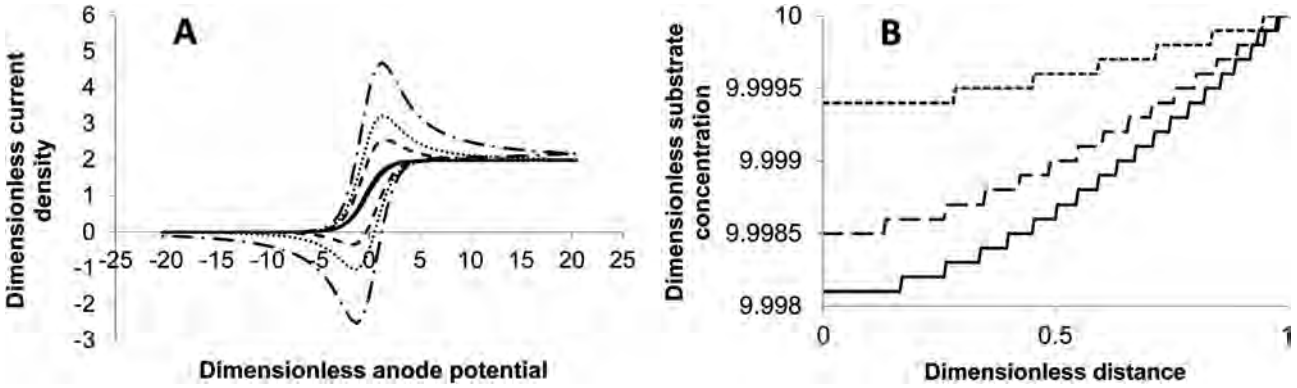

Fig. 9 Electron transport coupled with a Michaelis–Menten-type kinetics term; (A) cyclic voltammogram obtain for Da = 1 at scan rates ($\bar{v}$) = 1 (straight line), 20 (dashed line), 40 (dotted line) and 100 (dotted-dashed line); (B) dimensionless concentration profile of the substrate in the diffusion layer ($0 < \delta < 1$) for Da = 1, $\bar{v} = 1$ at potentials ($\bar{E}$) of −2 (straight line), 2 (dashed line) and 20 (dotted line).

5. Experimental

The partial derivative equations were solved numerically with the Matlab software using the "pdepe" module. The space and time grids of 200 steps each were designed with the "linspace" function.

6. Conclusions

The too straightforward interpretations of the J_{peak} *vs.* v^{α} relationship with $\alpha = 1$, supposed to indicate electron transport *via* an adsorbed species, and $\alpha = 0.5$, a diffusion-controlled process, must be used with care for the analysis of electron transport in EA biofilms. These basic rules were established for well-defined experimental conditions that are not always verified in the experimental investigations of EA biofilms. EA biofilms exhibit more complex and diverse experimental situations, which can lead to α values ranging from 1 to 0.5 for non-turnover CV, and α varying from 1 to lower values than 0.5 for catalytic CV. The theoretical approach proposed here now gives theoretical support to explain the various α values that have been reported in the literature. From the rigorous framework proposed here, simple rules were established in Sections 3.4 and 4.3, and summarized in Table 2 to enable CV analysis to deploy its full potential in the domain of EA biofilms. Moreover, this work should now allow transient CV analysis to be broadened to catalytic conditions, which has not been done so far in the EA biofilm area.

Table 2 Overview of the variation of the α exponent in the J_{peak} *vs.* v^{α} relationship

Value of α	Characterization of the electron transport (ET) process	Comments
Non-turnover condition (no substrate)		
1	ET system confined in the biofilm	Current falls close to zero at high potentials on CV (Fig. 5A); thin and/or efficient EA biofilm (low δ and/or high D_{app}) and/or low potential scan rate; eqn (44) can be used
Between 1 and 0.5	ET system confined in the biofilm	No diffusion-limited current on the CV; the EA biofilm becomes thicker and/or less efficient as α decreases
0.5	Mediator freely diffusing to/from the bulk solution	A diffusion-limited current is observed on CV curves (Fig. 3A)
	Or	Suggestion: Repeat CV in fresh solution that does not contain mediators to differentiate the two mechanisms
	ET system confined in the biofilm	No diffusion-limited current on the CV but the current may remain far from zero at the highest potentials (Fig. 5A) thick and/or poorly efficient EA biofilms (large δ and/or low D_{app}) and/or high scan rates
Catalytic condition assuming that the ET system is confined inside the biofilm		
Around 1	ET faster than metabolic reaction	In all the cases a limiting catalytic current is observed on the CV curves (Fig. 6), which can be calculated by eqn (67). The limiting catalytic current remains unchanged up to higher scan rates when the metabolic rate increases
Around 0.5	ET and metabolic reaction rates of similar orders of magnitude	
Lower than 0.5	Metabolic rate faster than ET	

Abbreviations

[Ac]	Concentration of the substrate, here acetate (mol m^{-3})
$[Ac]^B$	Concentration of the substrate, here acetate in the bulk (mol m^{-3})
D_X	Diffusion coefficient of the X species (m^2 s^{-1})
D_{app}	Apparent diffusion coefficient of the redox mediator in the biofilm (m^2 s^{-1})
Da	Damköhler number for a first-order metabolic reaction, defined in eqn (63)
Da′	Damköhler number for a Michaelis–Menten metabolic reaction, defined in eqn (79)
E	Potential (*V vs.* a reference electrode)
E_{ini}	Initial potential in CV (*V vs.* a reference electrode)
$E^{0\prime}$	Formal potential (*V vs.* a reference electrode)
F	Faraday's constant ($F = 96485$ C mol^{-1})
J	Current density (A m^{-2})
J_{lim}	Limiting catalytic current density (A m^{-2})
J_{peak}	current density at the current peak (A m^{-2})
k	Rate constant for electron release from the microbial cell (mol^{-1} m^3 s^{-1})
k_{cat}	Rate constant for microbial oxidation of acetate (mol^{-1} m^3 s^{-1})
K_M	Michaelis–Menten constant expressing affinity of the microbial cells for acetate (mol m^{-3})
$[Med_T]$	Total concentration of the redox mediator (oxidized and reduced species) (mol m^{-3})
$[Mic_{ox}]$, $[Mic_{red}]$, $[Mic_{ox}\text{–}Ac^-]$, $[Mic_T]$	Concentration of microbial species (mol m^{-3})
n	Number of exchanged electrons
[Ox]	Concentration of the oxidized form of the redox compound (diffusible or immobilized mediator) (mol m^{-3})
R	Universal gas constant (8.314 J mol^{-1} K^{-1})
Rate	Rate of electron release by the microbial cells (mol m^{-3} s^{-1})
Red	Concentration of the reduced form of the redox compound (diffusible or immobilized mediator) (mol m^{-3})
t	Time (s)
v	Potential scan rate (V s^{-1})
$v_{threshold}$	Potential scan rate above which the stationary response shifts to transient responses (V s^{-1})
x	Distance from the electrode surface (m)
α	Exponent of the scan rate v in the relationship J_{peak} *vs.* v
δ	Biofilm thickness or diffusion layer thickness for the Nernst-diffusion model (m)

Acknowledgements

This work was part of the "Défi H12" project financially supported by the "Bioénergies" programme of the French "Agence Nationale de la Recherche" (ANR-09-BioE-010 DéfiH12).

Notes and references

1 H. A. Videla and L. K. Herrera, *Int. Microbiol.*, 2005, **8**, 169–180.
2 I. B. Beech, J. A. Sunner and K. Hiraoka, *Int. Microbiol.*, 2005, **8**, 157–168.
3 B. Erable, D. Feron and A. Bergel, *ChemSusChem*, 2012, **5**, 975–987.
4 A. P. Borole, G. Reguera, B. Ringeisen, Z.-W. Wang, Y. Feng and B. H. Kim, *Energy Environ. Sci.*, 2011, **4**, 4813–4834.
5 D. Pant, A. Singh, G. Van Bogaert, S. I. Olsen, P. S. Nigam, L. Dielsa and K. Vanbroekhoven, *RSC Adv.*, 2012, **2**, 1248–1263.
6 T. H. J. A. Sleutels, A. Ter Heijne, C. J. N. Buisman and H. V. M. Hamelers, *ChemSusChem*, 2012, **5**, 1012–1019.
7 C. I. Torres, A. K. Marcus, P. Parameswaran and B. E. Rittman, *Environ. Sci. Technol.*, 2008, **42**, 6593–6597.
8 H. V. M. Hamelers, A. ter Heijne, N. Stein, R. A. Rozendal and C. J. N. Buisman, *Bioresour. Technol.*, 2011, **102**, 381–387.
9 X. Zhu, M. D. Yates and B. E. Logan, *Electrochem. Commun.*, 2012, **22**, 116–119.
10 E. Marsili, J. B. Rollefson, D. B. Baron, R. M. Hozalski and D. R. Bond, *Appl. Environ. Microbiol.*, 2008, **74**, 7329–7337.
11 A. Jain, X. Zhang, G. Pastorella, J. O. Connolly, N. Barry, R. Woolley, S. Krishnamurthy and E. Marsili, *Bioelectrochemistry*, 2012, **87**, 28–32.
12 S. Srikanth, E. Marsili, M. C. Flickinger and D. R. Bond, *Biotechnol. Bioeng.*, 2008, **99**, 1065–1073.
13 M. Sharma, N. Aryal, P. M. Sarma, K. Vanbroekhoven, B. Lal, X. Dominguez Benetton and D. Pant, *Chem. Commun.*, 2013, **49**, 6495–6497.
14 H. Richter, K. P. Nevin, H. F. Jia, D. A. Lowy, D. R. Lovley and L. M. Tender, *Energy Environ. Sci.*, 2009, **2**, 506–516.
15 S. M. Strycharz, A. P. Malanoski, R. M. Snider, H. Yi, D. R. Lovley and L. M. Tender, *Energy Environ. Sci.*, 2011, **4**, 896–913.
16 K. P. Katuri, P. Kavanagh, S. Rengaraj and D. Leech, *Chem. Commun.*, 2010, **46**, 4758–4760.
17 A. A. Carmona-Martinez, F. Harnisch, L. A. Fitzgerald, J. C. Biffinger, B. R. Ringeisen and U. Schröder, *Bioelectrochemistry*, 2011, **81**, 74–80.
18 K. Fricke, F. Harnisch and U. Schröder, *Energy Environ. Sci.*, 2008, **1**, 144–147.

19 Y. Liu, H. Kim, R. Franklin and D. R. Bond, *Energy Environ. Sci.*, 2010, **3**, 1782–1788.

20 E. Marsili, J. Sun and D. R. Bond, *Electroanalysis*, 2010, **22**, 865–874.

21 K. P. Katuri, S. Rengaraj, P. Kavanagh, V. O'Flaherty and D. Leech, *Langmuir*, 2012, **28**, 7904–7913.

22 A. J. Bard and L. R. Faulkner, *Electrochemical Methods*, John Wiley & Sons, New York, 2nd edn, 2001, vol. 1, ch. 6, p. 231.

23 A. J. Bard and L. R. Faulkner, *Electrochemical Methods*, John Wiley & Sons, New York, 2nd edn, 2001, vol. 1, ch. 11, p. 432.

24 K. Rabaey, N. Boon, M. Hofte and W. Verstraete, *Environ. Sci. Technol.*, 2005, **39**, 3401–3408.

25 A. K. Shukla, P. Suresh, S. Berchmans and A. Rajendran, *Curr. Sci.*, 2004, **87**, 455–468.

26 E. Marsili, D. B. Baron, I. D. Shikhare, D. Coursolle, J. A. Gralnick and D. R. Bond, *Proc. Natl. Acad. Sci. U. S. A.*, 2008, **105**, 3968–3973.

27 C. I. Torres, A. K. Marcus, P. Parameswaran and B. E. Rittmann, *Environ. Sci. Technol.*, 2008, **42**, 6593–6597.

28 A. K. Marcus, C. I. Torres and B. E. Rittmann, *Biotechnol. Bioeng.*, 2007, **98**, 1171–1182.

29 C. I. Torres, A. K. Marcus, H. S. Lee, P. Parameswaran, R. Krajmalnik-Brown and B. E. Rittmann, *FEMS Microbiol. Rev.*, 2010, **34**, 3–17.

30 S. R. Crittenden, C. J. Sund and J. J. Sumner, *Langmuir*, 2006, **22**, 9473–9476.

31 D. R. Lovley, *Curr. Opin. Biotechnol.*, 2008, **19**, 564–571.

32 A. J. Bard and L. R. Faulkner, *Electrochemical Methods*, John Wiley & Sons, New York, 2nd edn, 2001, vol. 1, ch. 9, p. 335.

33 O. V. Klymenko, R. G. Evans, C. Hardarcre, I. B. Svir and R. G. Compton, *J. Electroanal. Chem.*, 2004, **571**, 211–221.

34 A. J. Bard and L. R. Faulkner, *Electrochemical Methods*, John Wiley & Sons, New York, 2nd edn, 2001, vol. 1, ch. 11, p. 452.

35 R. Devaux, A. Bergel and M. Comtat, *AIChE J.*, 1995, **41**, 1944–1954.

36 S. Bacha, M. Montagne and A. Bergel, *AIChE J.*, 1996, **42**, 2967–2976.

37 T. H. Pham, N. Boon, P. Aelterman, P. Clauwaert, L. De Schamphelaire, L. Vanhaecke, K. De Maeyer, M. Höfte, W. Verstraete and K. Rabaey, *Appl. Microbiol. Biotechnol.*, 2008, **77**, 1119–1129.

38 I. Katakis and A. Heller, *Anal. Chem.*, 1992, **64**, 1008–1013.

39 E. V. J. M. Saveant, *Electrochim. Acta*, 1965, **10**, 905–920.

40 I. H. Segel, *Enzyme Kinetics, Behaviour and Analysis of Rapid Equilibrium and Steady-state Enzyme Systems*, John Wiley & Sons, New York, 1st edn, 1993, vol. 1, ch. 9, p. 505.

41 D. Pocaznoi, A. Calmet, L. Etcheverry, B. Erable and A. Bergel, *Energy Environ. Sci.*, 2012, **5**, 9645–9652.